An Evolution of the Asian Summer Monsoon Associated with Mountain Uplift—Simulation with the MRI Atmosphere-Ocean Coupled GCM—

Manabu ABE

Doctoral program in Geoscience, University of Tsukuba, Tsukuba, Japan

Akio KITOH

Meteorological Research Institute, Tsukuba, Japan

and

Tetsuzo YASUNARI[1]

Institute of Geoscience, University of Tsukuba, Tsukuba, Japan

(Manuscript received 10 September 2002, in revised form 3 April 2003)

Abstract

Using the MRI global atmosphere-ocean coupled general circulation model, we had six simulations with different mountain heights, i.e., 0% (M0), 20% (M2), 40% (M4), 60% (M6), 80% (M8), and 100% (M, control run) of the present global orography, respectively, to study climate changes due to progressive mountain uplift. The changes of the Asian summer monsoon, with progressive mountain uplift is studied in this paper.

An active convection region extends with mountain uplift to form a moist climate in South and East Asia. Monsoon circulation such as low-level westerly, and upper-level anticyclonic circulation, is also enhanced with mountain uplift. The increase in precipitation, and the enhancement of southwesterly, in the later stages of the mountain uplift, appear only over India and the south and southeastern slope of the Tibetan Plateau. Over the coastal region of Southeast and East Asia, where the maximum precipitation appears in M0, precipitation decreases gradually with mountain uplift, and the southwesterly in the later stages becomes weaker. In the connection with these changes, surface heat flux changes remarkably over moist Asia in the earlier stages of mountain uplift, compared with that in the later stages. The intensity of the Indian, Southeast Asian, and East Asian monsoon was investigated with indices which are defined by area mean precipitation. The Indian monsoon becomes strong gradually with mountain uplift; particularly, in the later stages, the remarkable enhancement is found. The intensity of the South Asian monsoon is the strongest in M4. Thus, in the later stages of mountain uplift, that becomes weaker in association with the northwestward migration of the convective activity. Although the East Asian monsoon is enhanced gradually with mountain uplift, the enhancement in the earlier stages

Corresponding author and present affiliation: Manabu Abe, Hydrospheric Atmospheric Research Center, Nagoya University, Furo-cho, Chikusa-ku, Nagoya, 464-8601, Japan.
E-mail: mabe@ihas.nagoya-u.ac.jp

1 Present affiliation: Hydrospheric Atmospheric Research Center, Nagoya University, Nagoya, Japan.

is larger than that in the later stages. In the equatorial Indian Ocean, SST also increases with mountain uplift, resulting in the increase in precipitation. The increase in SST results from the change of the ocean surface dynamics due to the enhanced monsoon circulation. This result could not be obtained if CGCM was not used in this study.

1. Introduction

Large-scale orography, such as the Tibetan Plateau and the Rocky mountains, plays important roles to form the present global climate system (Kutzbach et al. 1993). The large-scale orography has dynamical and thermodynamical effects to the atmosphere, which in turn influences the ocean circulation through the atmosphere-ocean interaction. For the Asian summer monsoon, the Tibetan Plateau is very important to induce and maintain the monsoon circulation, but the effects and the role of the Tibetan Plateau is not understood fully on the intraseasonal, interseasonal, annual, and interannual variability in present. Furthermore, the mountain uplift occurred in the geological history must be one of the cause of the past climate change (Kutzbach et al. 1993).

Many previous studies have investigated the effect of mountains on the Asian summer monsoon using a climate model. Most of the previous model studies conducted a comparison between mountain-run (M) and no-mountain run (NM) using an atmospheric general circulation model (AGCM) (Manabe and Terpstra 1974; Hahn and Manabe 1975; Tokioka and Noda 1986; Broccoli and Manabe 1992), or an atmosphere-ocean coupled GCM (CGCM) (Kitoh 1997; Kitoh 2002). However, these studies could not reveal to what degree the change of mountain height affect a climate and monsoon. It can also be postulated that the effect of mountains does not necessarily change linearly with increasing mountain altitudes. Kutzbach et al. (1989), by using AGCM conducted three experiments, i.e., no-mountain run (NM), half-mountain run (HM), and mountain run (M), to investigate how the components of monsoon changed linearly, or non-linearly, associated with progressive mountain uplift. Their study concluded that atmospheric heating rates, mid-tropospheric vertical motion, and upper-tropospheric planetary wave amplitude varied approximately linearly with progressive mountain uplift. However, as the change from NM to HM, and that from HM to M, were not investigated in their study, experimental design with the three stages of mountain uplift in their study was not sufficient to investigate the commencement of the Asian summer monsoon as is in present or the detailed change in a climate by progressive mountain uplift. Thus, it is necessary to study the evolution of the Asian summer monsoon considering the changes among the three stages set in Kutzbach et al. (1989). Recently, in Liu and Yin (2002), 11 experiments, in which the different heights of the Tibetan Plateau were prescribed, were conducted to examine the impact of progressive uplift of the Tibetan Plateau on the evolution of the East Asian monsoon using AGCM. However, their study did not take account of the ocean circulation changes due to mountain uplift. The Asian summer monsoon may play an active role in the interannual variability of the atmosphere-ocean coupled system in the tropical Pacific through the east-west circulation (Yasunari 1990). Kutzbach et al. (1993) and Kitoh (1997) have made experiments using an atmospheric general circulation model with a 50 m slab ocean model. In their studies, sea surface temperature (SST) distribution near the continents in mountain run was different from that in no-mountain run. Moreover, Kitoh (2002) investigated the surface climate changes with mountain uplift using CGCM. Kitoh (2002) showed the decrease in SST with mountain uplift, particularly over the subtropical eastern Pacific ocean, due to less shortwave radiation into surface by increased low-level clouds and more evaporation by an enhanced trade wind. In the real climate system, the presence of mountain is important to form SST distribution, and the oceanic circulation as well as the atmospheric circulation. Although studies have been made on the effects of mountains using GCM, there has been few studies using CGCM that tried to reveal the effects of mountains taking account of mountain height on the climate system including the ocean system. The changing oceanic general circulation

should be considered for fully understanding the effects of orography on climate formation. Thus, systematic experiments using the Meteorological Research Institute (MRI) CGCM are made to investigate the climate changes due to progressive mountain uplift more in detail.

For geological climate changes related to mountain uplift, it is difficult to deduce the influence of mountain uplift only from geological evidences. Thus, the quantitative evaluation of climate change related to mountain uplift using a climate model can supply significant information and theoretical interpretations for the past climate changes due to mountain uplift.

In this paper, we focus on the changes in the Asian summer monsoon. Since CGCM is used in this study, experiments in this study differ essentially from experiments in Liu and Yin (2002) using AGCM, although the different heights of mountain were also set in this study. Further, our preparing paper investigates the influences of mountain uplift to the Pacific and Indian ocean sector. Although the global orography is changed in this study, other experiments to examine the sole effects of the Tibetan Plateau, and the Rocky mountains are also conducted.

Section 2 describes the model and experimental design. The changes of the Asian monsoon with progressive mountain uplift are shown in Section 3. Section 4 shows the change in the intensity of the Asian summer monsoon indicated by indices.

2. Model and experimental design

The model used in this study is a global ocean-atmosphere coupled general circulation model which is a grid point model developed at MRI (MRI-CGCM1, Tokioka et al. 1995). The horizontal resolution of the atmospheric model is 5° longitude and 4° latitude and the vertical resolution is 15 layers with an atmospheric top at 1 hPa. The calculations of shortwave radiation are based on the parameterization of Lacis and Hansen (1974). Rayleigh scattering and absorption by ozone and water vapor are calculated. Longwave radiation is calculated based on the multiparameter random model of Shibata and Aoki (1989). The model uses a parameterization of the modified Arakawa-Schubert penetrative cumulus convection (Tokioka et al. 1988). The calculation of orographic gravity-wave drag follows Palmer et al. (1986). The land surface has 4 layers with a bottom at 10 m depth. Ground temperature, ground wetness and frozen soil moisture are prognostic variables calculated at each level of the land surface. The effects of vegetation are not explicitly considered on the land surface processes. The details of the performance of the AGCM are described by Kitoh et al. (1995).

The global oceanic model is developed at MRI (Nagai et al. 1992), which contains 21 vertical levels, 11 of which are located between 300 m depths and the oceanic surface. A realistic bottom topography is included in the model. The ocean general circulation model (OGCM) has a resolution of 2.5° longitude and 2.0° latitude. To resolve the equatorial waves and the narrow equatorial upwelling region sufficiently, however, non-uniform meridional resolution from 0.5° to 2.0° is introduced within the equatorial region of 12°S–12°N. The simulation of the oceanic mixed layer is calculated following the Mellor-Yamada level 2 turbulence closure scheme.

In order to produce realistic SST, and sea surface salinity fields, the flux adjustment for surface energy and water flux is operated. Although the original model predicts sea ice concentration and its depth, in this study, we specified the sea ice conditions in their monthly climatology based on the observations.

Figure 1 shows the seasonal mean distribution of precipitation and SST during June–August in control run (M). The SST pattern is reproduced reasonably since the flux adjustment is working well. A warm pool in the western Pacific, and a cold tongue in the eastern Pacific are well simulated. Large-scale precipitation distribution agrees with the observed climatology. There are also the Intertropical Convergence Zone (ITCZ), and the South Pacific Convergence Zone (SPCZ) in the Pacific.

The results of the climatological state and interannual variability of the Asian monsoon and atmosphere-ocean system over the Pacific in this model were investigated by Kitoh et al. (1999). In their study, the overall features of the model climatology and variability of the Asian summer monsoon in the CGCM were found to be close to the observed one. The simulated SST and its variability in the CGCM showed some bias compared to the observation.

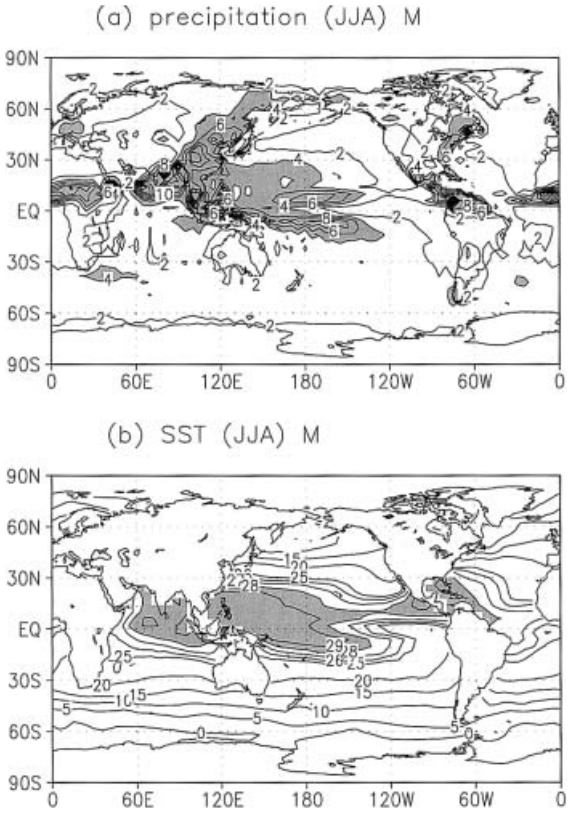

Fig. 1. (a) Seasonal mean precipitation during June–August in M. Unit is mm day^{-1} and the contour interval is 2 mm day^{-1}. The values above 4 mm day^{-1} are shaded. (b) Seasonal mean SST during June–August in M. Unit is °C and the contour interval is 1°C. The values above 28°C are shaded.

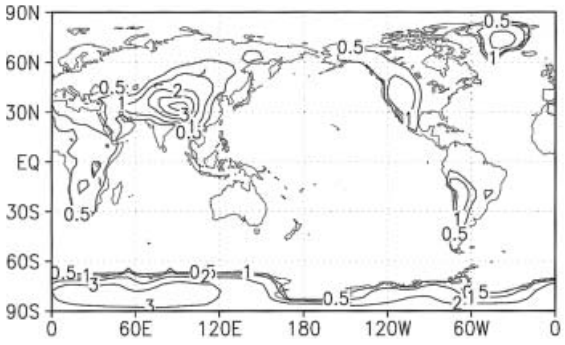

Fig. 2. Orography used in the control run (M). Unit is ×1000 m and the contours are 0.5, 1, 2, 3, and 4.

The seasonal change of wind direction and convections over the monsoon region in the model agrees well with those of the observation. The interdecadal variability in the Pacific sector in the model was found to be realistic (Yukimoto et al. 1996).

In order to investigate the evolution of the Asian summer monsoon with progressive mountain uplift, six runs were performed, which were integrated for 50 years respectively. Control run with the standard present orography is designated as the M run. The top elevation of the Tibetan Plateau is 4400 m in M (Fig. 2). M0 run, M2 run, M4 run, M6 run and M8 run were conducted under the boundary conditions of 0%, 20%, 40%, 60%, and 80% of the global orography in M, respectively. Land-sea distribution is the same in all the runs. All the runs started from the same initial condition with the orography height in M run. In order to avoid a calculation error due to a rapid change of the boundary condition, the height of orography in runs, except M run, was decreased 10% of standard present orography by a month. After the mountain height in each run reached the designed height, the integrations were continued with the fixed mountain height. Since the true climatological states of SST, and surface salinity in runs, except M run, are not known, the adjustment values for flux adjustment in M were regarded as the deficient values for exchanges of heat energy and fresh water flux between the atmosphere and the ocean in the CGCM in this study. Thus, the flux adjustment with the same adjustment data in M was also operated in other runs.

Figure 3 shows the time series of annual mean sea water temperature averaged vertically between surface and 300 m depth over the equatorial Pacific Ocean (150°E–80°W, 10°S–10°N). The averaged temperature in runs, except M, also reaches equilibrium within about 10 years, although its interannual variability appears for 50 years in all the runs.

M0 run has a flat surface everywhere and is the same as NM run in Kitoh (2002). Seasonal mean data averaged for the last 30 years (21–50) integrations are used for analysis in this study.

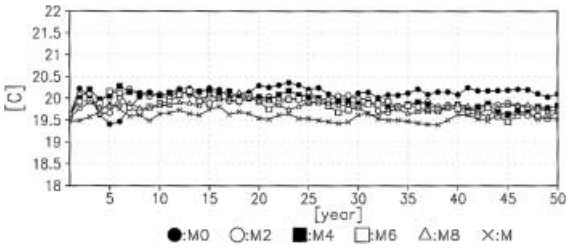

Fig. 3. Time series of annual mean sea water temperature averaged vertically between surface and 300 m depth in the equatorial Pacific (150°E–80°W, 10°S–10°N). Unit is °C.

3. Changes with mountain uplift

3.1 Rainfall and low-level circulation

Figure 4 shows the distribution of precipitation and wind at 850 hPa averaged from June to August over Asia in M0, M2, M4, M6, M8, and M. The difference of precipitation, and wind at 850 hPa between M2 and M0, M6 and M4, and, M and M8, are shown in Fig. 5. Precipitation in M0 (with land-sea distribution, but without mountains) is shown in Fig. 4a. Although all mountains are removed, active convections are found from west Africa through the Indochina Peninsula to the East China Sea in M0, which can be identified as summer monsoon rainfall. A convection center over Asia in M0 is located over the Bay of Bengal, the Indochina Peninsula and the Arabian Sea with precipitation above 10 mm day^{-1}. Monsoon westerly centered at 10°N also appears over South Asia in M0. The maximum zonal wind velocity is located over the Bay of Bengal in M0, which coincides with the center of active convection in M0. Further southwesterly from South Asia blows through Japan to the North Pacific. Over the equatorial Indian Ocean, cross-equatorial wind from the southern hemisphere to the northern hemisphere appears. However, the Somali Jet is not found clearly, but the maximum meridional wind velocity is located over the eastern Indian Ocean. Further, the small amount of precipitation is seen in northern India, where northerly blows to converge with southwesterly at about 10°N to form monsoon westerly in M0. Besides, there is relatively strong mid-latitude westerly over 40°N–60°N of Eurasia in M0. Precipitation over the land within 20°N–40°N, where the Tibetan Plateau and a dry climate region are located in the present, is also small. In the region over and around the Caspian Sea, however, the climate is more rainy compared to that south of there.

In M2 (Fig. 4b), some differences from M0 appear. Precipitation in M2 increases in eastern China, to the east of 70°E, and Mongolia, compared with that in M0 (Fig. 5a). One can find that the area of precipitation above 4 mm day^{-1} extends into the interior in East Asia, as Fig. 5a shows positive values above 1 mm day^{-1} in the whole of East Asia. Furthermore, the increase in precipitation is found over the Arabian Sea, and the Bay of Bengal and Myanmar region in Fig. 5a. Southwesterly over the Arabian Sea and cross-equator flow over the western Indian Ocean become strong, and southwesterly over northwestern India is also stronger in M2 than in M0. The changes of flow at low-level enhance water vapor flux into the land area over South and East Asia to increase precipitation. The precipitation increase, and the circulation changes from M0 to M4, also become more obvious in regions where the increase in precipitation is found in M2. The migration of active convections from the Bay of Bengal to northern India is also found over northwest India from M0 to M4. Over the western Tibetan Plateau, northwesterly in M0 changes to northerly in M4, which flows into northern India as northwesterly. Further, moist southwesterly also intrudes into northern India and combines with dry northwesterly over India, which may be related to the increase in precipitation over India.

In M6 (Fig. 4d), a significant difference from M4 appears over the Bay of Bengal and the Indochina Peninsula, where precipitation decreases (Fig. 5b). In northern India, the area of precipitation above 4 mm day^{-1} continues to expand from southeast to northwest to result in increased precipitation (Fig. 5b).

In M8 (Fig. 4e) and M (Fig. 4f), precipitation decreases further over the Bay of Bengal and East Asia (Fig. 5c). In addition, the decrease of precipitation is found over the Arabian Sea, and the South China Sea from M8 to M. On the other hand, the northwestward migration of active convection continues in northwestern

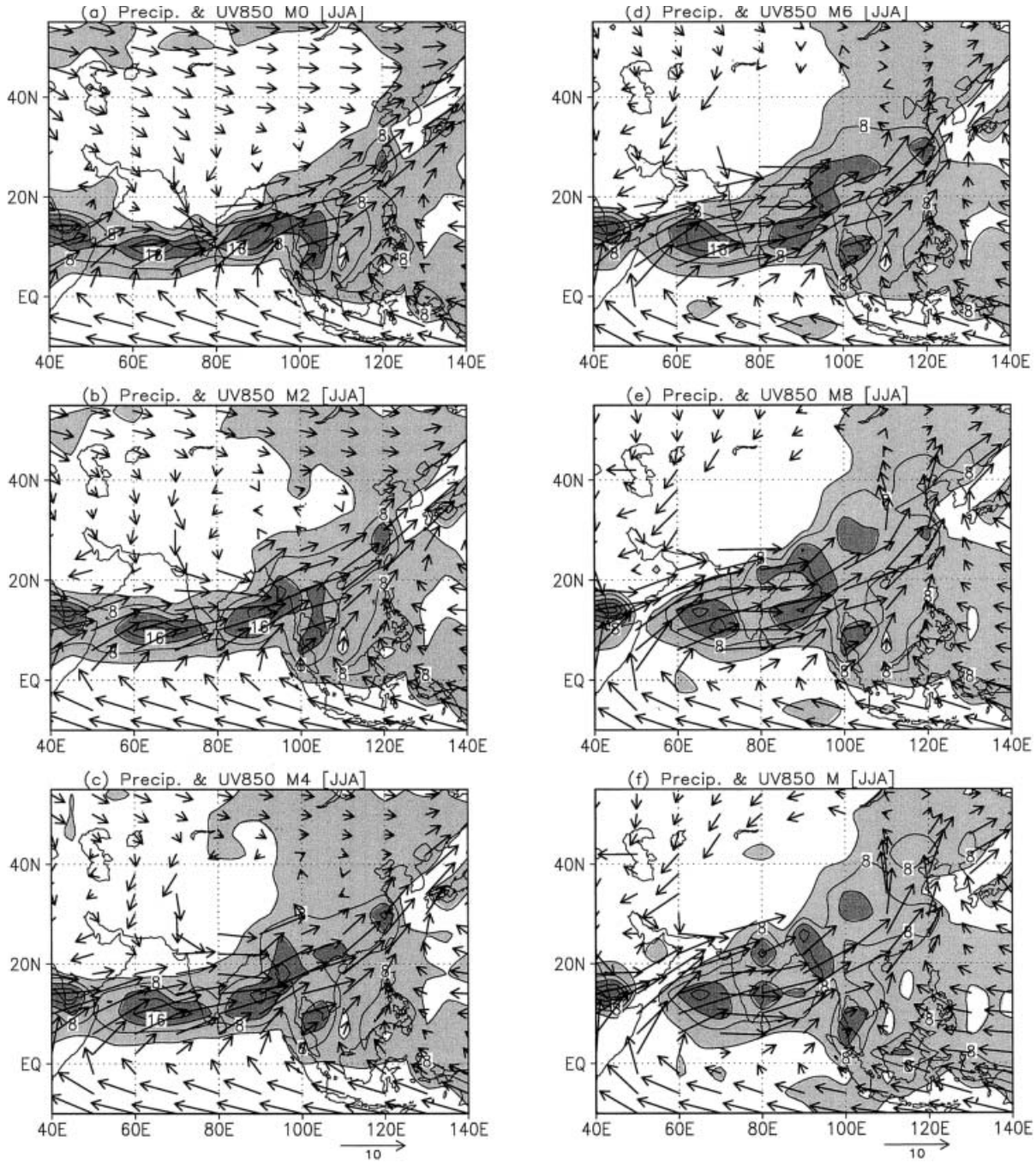

Fig. 4. Seasonal mean precipitation and wind at 850 hPa during June–August in each run. Units of precipitation are mm day^{-1} and the contour interval is 4 mm day^{-1}. The values above 4 mm day^{-1} are shaded. Units of wind are m sec^{-1}.

India in M8 and M. Thus, an active convection region extends northward in India and the Bay of Bengal region with mountain uplift. From M8 to M, precipitation increases in the dry region of northwestern India, and the west of the Tibetan Plateau (Fig. 5c). Monsoon westerly over South Asia becomes stronger in M6 compared with that in M4 (Fig. 5b). The maximum

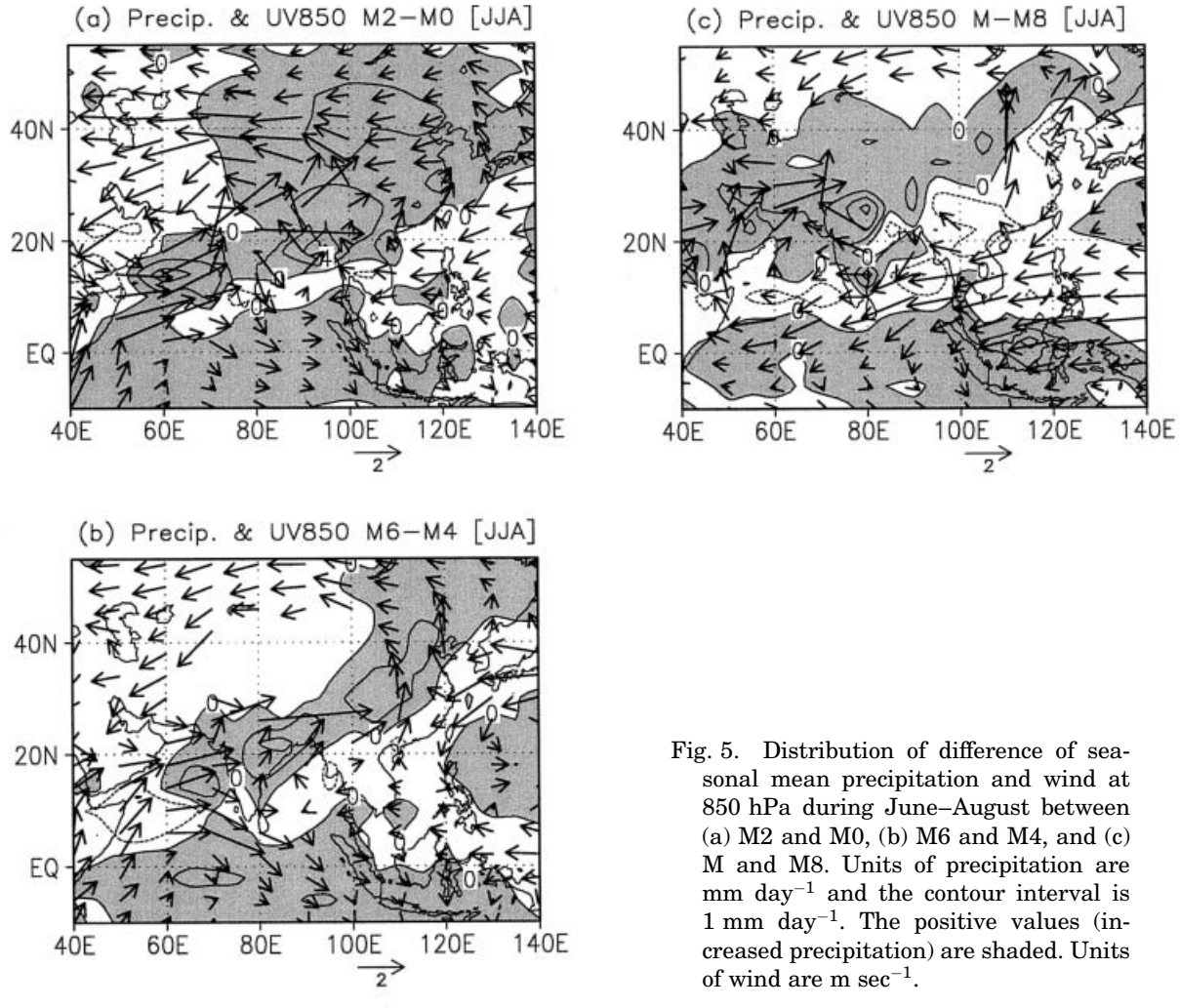

Fig. 5. Distribution of difference of seasonal mean precipitation and wind at 850 hPa during June–August between (a) M2 and M0, (b) M6 and M4, and (c) M and M8. Units of precipitation are mm day^{-1} and the contour interval is 1 mm day^{-1}. The positive values (increased precipitation) are shaded. Units of wind are m sec^{-1}.

wind speed of the monsoon westerly appears over the Arabian Sea in M6, while it is located over the Bay of Bengal in M0 (Fig. 6). Over the Bay of Bengal and the Indochina Peninsula, monsoon westerly becomes weak from M6 to M, which coincides with the decrease in precipitation, while it remains stronger and moves northward over the Arabian Sea. Figure 5c clearly shows westward wind anomalies from the Bay of Bengal through the Indochina Peninsula to the western Pacific. These wind anomalies indicate that monsoon westerly becomes weaker over the Bay of Bengal and the Indochina Peninsula, and that trade wind over the western Pacific is enhanced with mountain uplift. However, as shown in Fig. 5a and 5b, the westerly is enhanced over the north of the Bay of Bengal and the Indochina Peninsula from

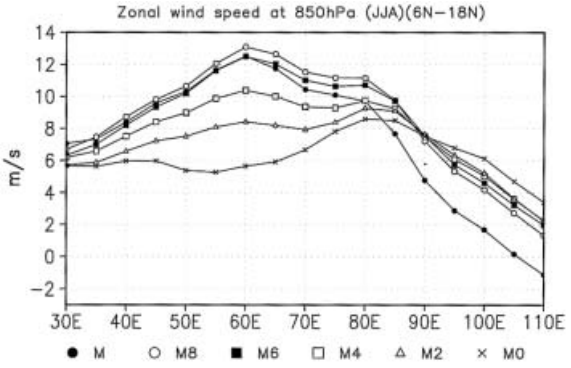

Fig. 6. Longitudinal distribution of seasonal mean zonal wind speed at 850 hPa during June–August averaged at 6°N–18°N in each run. Units is m s^{-1}.

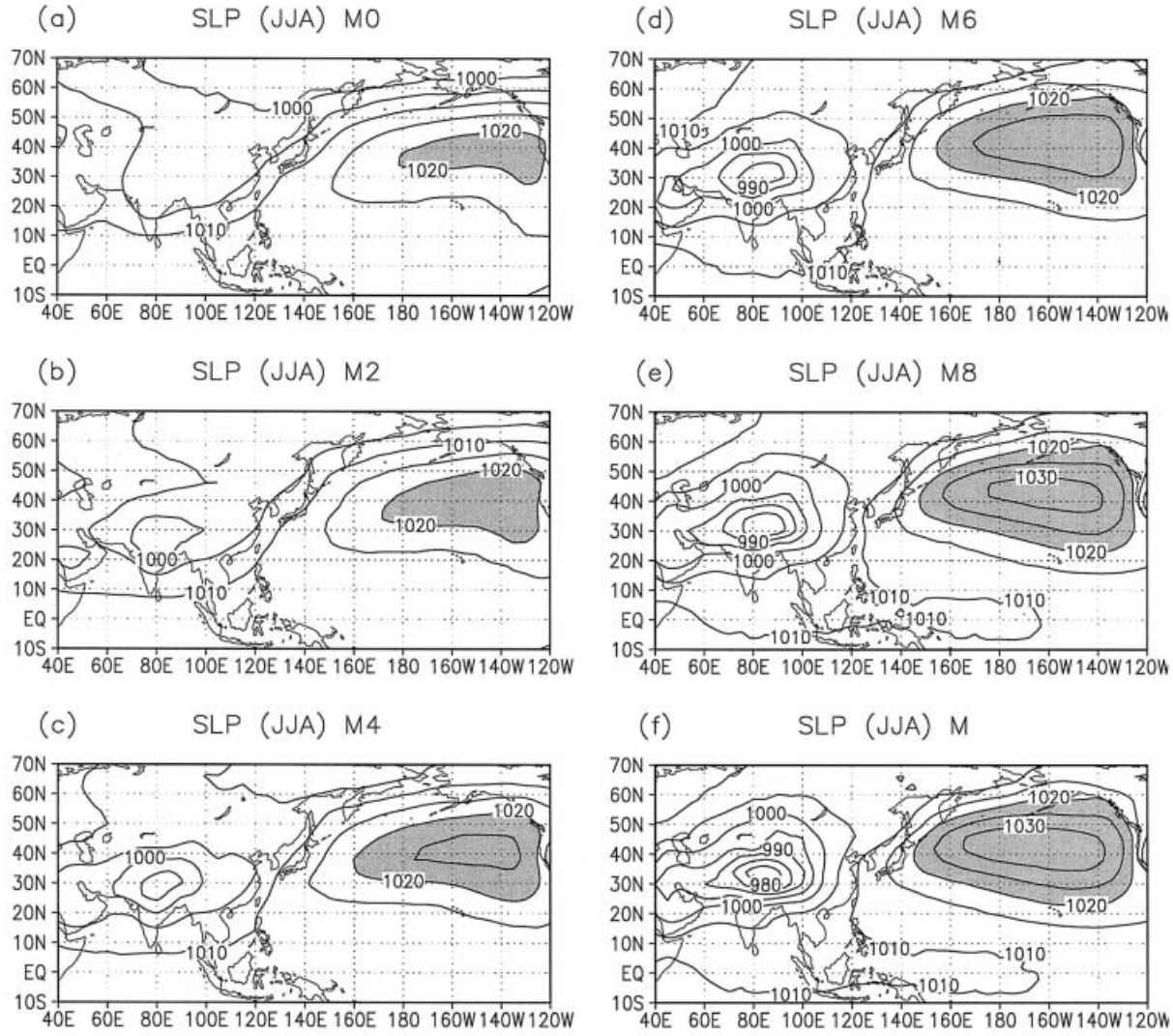

Fig. 7. Distribution of seasonal mean sea level pressure during June–August. Units are hPa. The values above 1020 hPa are shaded. For easy comparison, constant value is added for each experiment so that global mean values become the same as in M.

M0 to M8. These changes indicate the center of monsoon southwesterly moves northwestward into the interior with mountain uplift in Southeast and East Asia, coinciding with the northwestward expansion of an active convection region over Southeast and East Asia. Moreover, the flow over the Bay of Bengal has a strong northward component between M6 and M than that in the earlier mountain uplift stages. In this connection, the southwesterly in Northeast Asia moves into the interior, and flows from the Pacific through Japan become obvious between M6 and M, as the easterly wind anomaly from the Pacific exists over Japan as shown in Fig. 5c. These results over Southeast and East Asia may be related to an enhanced subtropical high over the Pacific. Figure 7 shows the seasonal mean sea level pressure during June–August in each run. Although the atmospheric mass was kept the constant value in all the runs, a reduction to the mean sea level pressure results in different global mean sea level pressure values. For easy comparison, a constant value is added to sea level pressure in each run so that the global mean values become the same as in M in the

figures. It is found obviously that the subtropical high over the Pacific is enhanced with mountain uplift. However, this change of the subtropical high is not affected only by Asian mountains, but also by mountains in other regions, e.g., the Rocky mountains (Hoskins 1996; Rodwell and Hoskins 2001). The enhanced subtropical high with mountain uplift causes a strong easterly wind from the western Pacific, particularly in M (Fig. 6). The enhanced subtropical high over the north Pacific results in a stronger trade wind over the Pacific and enhanced southeasterly from the western Pacific over Southeast Asia. The northwestward movement of monsoon southwesterly over East Asia may be also affected by the enhanced subtropical high with mountain uplift. Although the Somali Jet in the model intrudes into the East African continent, the enhancement of it with mountain uplift is found in Fig. 4. In brief, while the monsoon westerly is enhanced over South Asia from M0 to M4, the westerly from M6 to M is enhanced only over the Arabian Sea and the southern slope of the Tibetan Plateau, and weakened over the Bay of Bengal and the Indochina Peninsula.

Incidentally, weak westerly disappears over the land in the mid-latitude between M6 and M. The gradual extension of a small-precipitation region is also found in the north of Central Asia with mountain uplift. This result is consistent with a result by Broccoli and Manabe (1992), although precipitation increases from M8 to M in a part of Central Asia. In the equatorial Indian Ocean, precipitation increases with mountain uplift as shown by Fig. 5.

The northwestward extension of an active convection region is examined more clearly. Figure 8 shows the meridional distribution of precipitation averaged from 75°E to 85°E (line A-B drawn in Fig. 8a) in each experiment, and that in precipitation along line C-D drawn in Fig. 8a, which was drawn from Central Asia to Southeast Asia. In Fig. 8b, extremely heavy precipitation at 10°N in M0 is found. While the precipitation at 10°N decreases gradually with mountain uplift, precipitation at broad latitude of 14°N–26°N increases significantly. Further, the latitude at which the extreme increase of precipitation occurs among each consecutive mountain uplift, moves north within 14°N–26°N with progressive mountain uplift. In the later stages of mountain uplift, precipitation also increases particularly in India. In Fig. 8c, the maximum precipitation in M0 is located at 18°N. Precipitation over the north of the Indochina Peninsula and the southern slope of the Tibetan Plateau increases with mountain uplift. The precipitation over the Indochina Peninsula increases as whole from M0 to M4, particularly over the north of the peninsula. However, while the precipitation over the north of the peninsula and the slope of the Tibetan Plateau increases gradually from M6 to M, that over the Indochina Peninsula decreases, which indicates an active convection region intrudes northwestward into the interior in the later stages of mountain uplift.

3.2 Expansion of moist Asian climate toward the interior

Figure 9 shows the difference of mean sea level pressure (SLP) between the successive two stages (M2-M0, M4-M2, M6-M4, M8-M6, and M-M8). As stated above, since the atmospheric mass was kept the constant value in all the runs, a reduction to the SLP results in different global SLP values. The difference is calculated using the value which is modified by adding the constant value to SLP in each run so that its global mean value becomes the same as in M. In Fig. 9a and 9b, the decrease of SLP occurs over the Tibetan Plateau, and the west of the Tibetan Plateau including the Arabian Peninsula. On the other hand, over the east of the Tibetan Plateau, the small increase in SLP from M0 to M4 is found. From M6 to M, while SLP over the Tibetan Plateau and the west of the Plateau decreases gradually, the increase in SLP appears over India and the coastal region of East Asia. These SLP changes are consistent with the northwestward migration of southwesterly at 850 hPa over Southeast and East Asia with mountain uplift. While the southwesterly blowing from India to East Asia is enhanced over the slope of the Tibetan Plateau, the flow becomes weaker with mountain uplift in the southern side of the southwesterly. Therefore, precipitation over the southern part of the Bay of Bengal and the Indochina Peninsula, which is larger in M0, decreases with mountain uplift. Further, the southwesterly over the Arabian Sea is enhanced over the coastal region due to the gradual decrease in

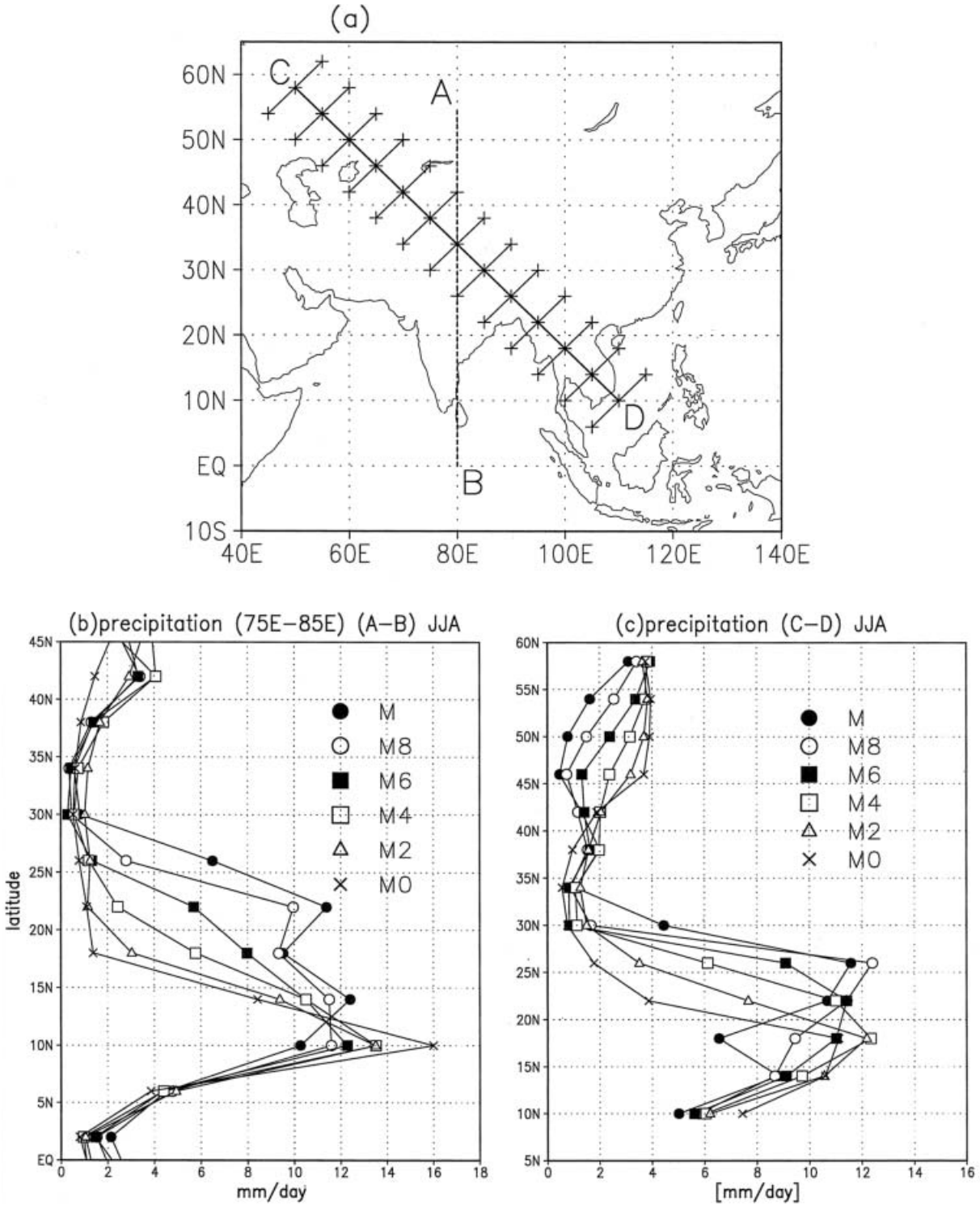

Fig. 8. The meridional distribution of seasonal mean precipitation during June–August averaged from 75°E to 85°E (A-B) in each run and that along C-D (from Central to Southeast Asia). The abscissa (ordinate) indicates precipitation (latitude). Units of precipitation are mm day^{-1}. In (c), the values on the line C-D, which are averaged for three grids (cross) on normal line to the line C-D, are plotted.

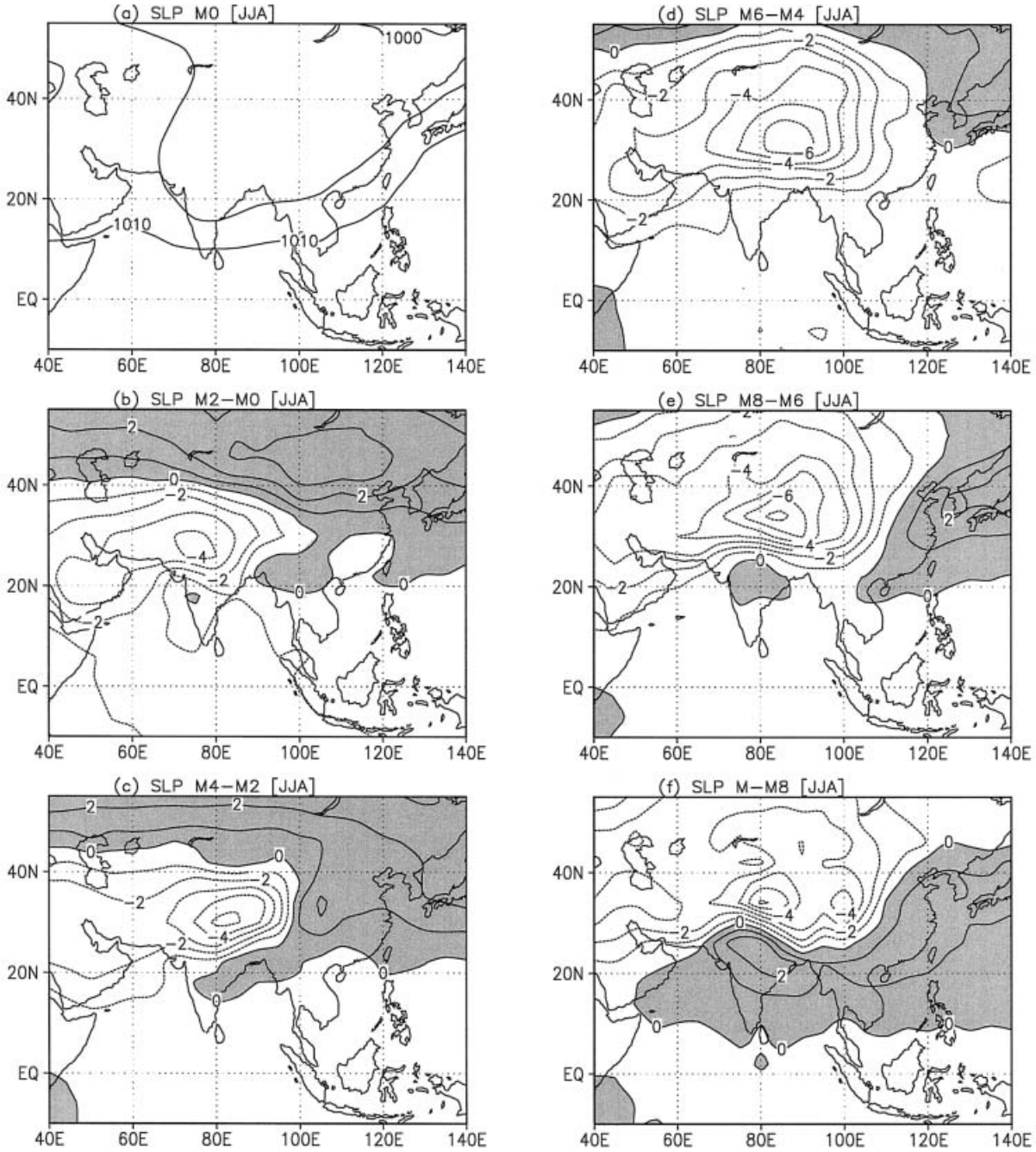

Fig. 9. (a) Seasonal mean sea level pressure (SLP) in M0 and the difference of seasonal mean SLP during June–August between (b) M2 and M0, (c) M4 and M2, (d) M6 and M4, (e) M8 and M6 and (f) M and M8. Units are hPa. The positive values are shaded. The difference is calculated using the value which is modified by adding the constant value to SLP in each run so that its global mean value becomes the same as in M.

SLP over the Arabian Peninsula and the Iran-Afghanistan region. The northward migration of the southwesterly in low-level also transports water vapor into India, resulting in the increase in precipitation over India.

The increase in SLP is found over East and South Asia (Fig. 9), coinciding with a region where surface air temperature decreases, and ground wetness increases over East and South Asia (Fig. 10). The large increase in ground

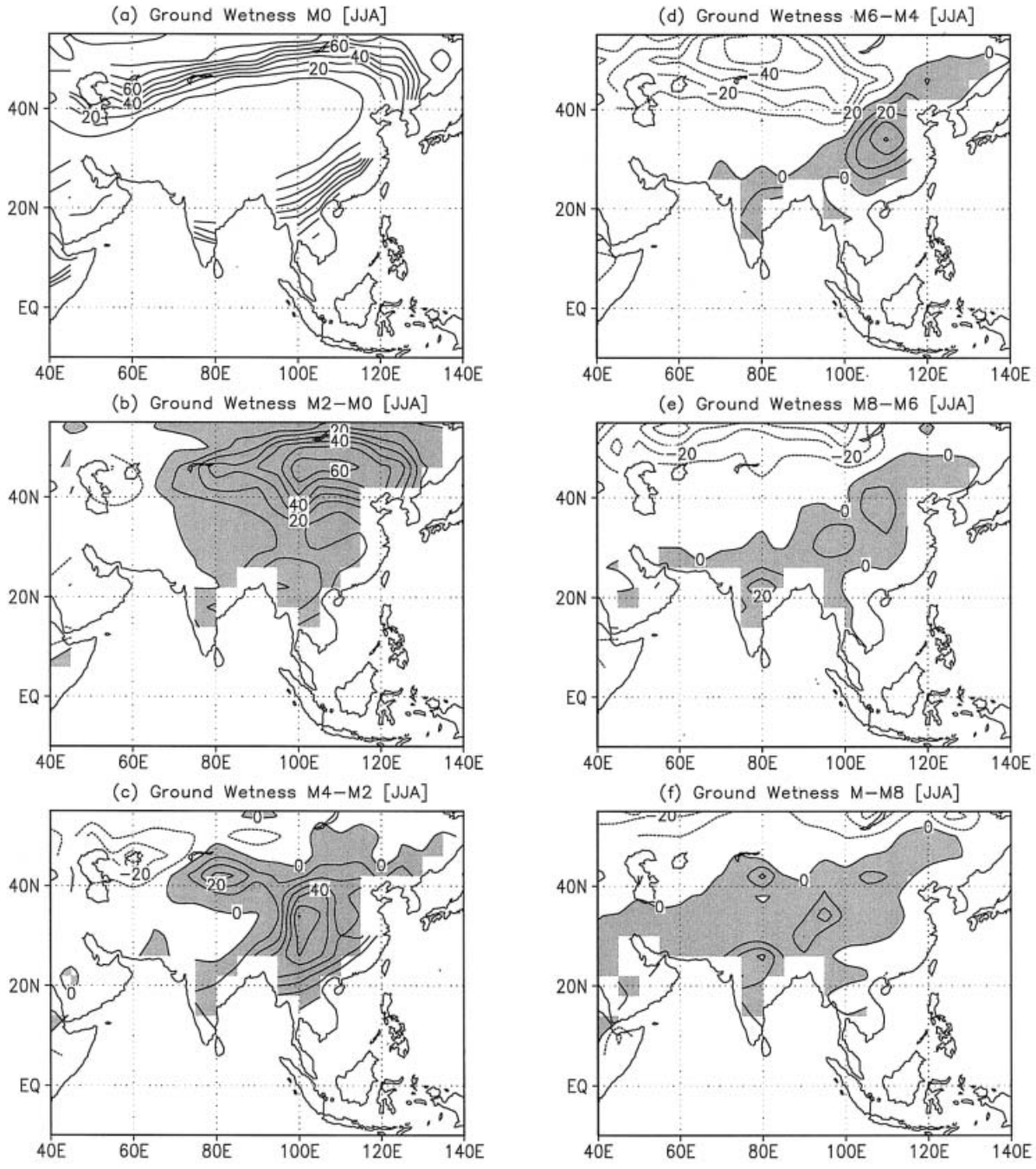

Fig. 10. (a) Seasonal mean ground wetness in M0 and the difference of seasonal mean ground wetness during June–August between (b) M2 and M0, (c) M4 and M2, (d) M6 and M4, (e) M8 and M6, and (f) M and M8. Units are %. The positive values are shaded.

wetness over Northeast and East Asia from M0 to M4, and that over North India from M8 to M are induced by the increase in precipitation. Therefore, the increase in SLP over moist Asia may be associated with reduced surface temperature by the increase in precipitation. In addition, the increase in SLP over the coastal region of East Asia may be affected by the enhanced subtropical high over the Pacific.

Figure 11 shows the difference of seasonal mean latent heat flux and sensible heat flux at surface between M2 and M0, M6 and M4, and M and M8, respectively. The changes of both fluxes with mountain uplift show the opposite sign in each other. Latent heat flux at surface increases over Northeast Asia and East Asia, particularly in Mongolia, while sensible heat flux at surface decreases about two third of the latent heat flux over the same region. Both heat flux changes also coincide with the increase of ground wetness. Further, the change of both heat flux in other stages of mountain uplift

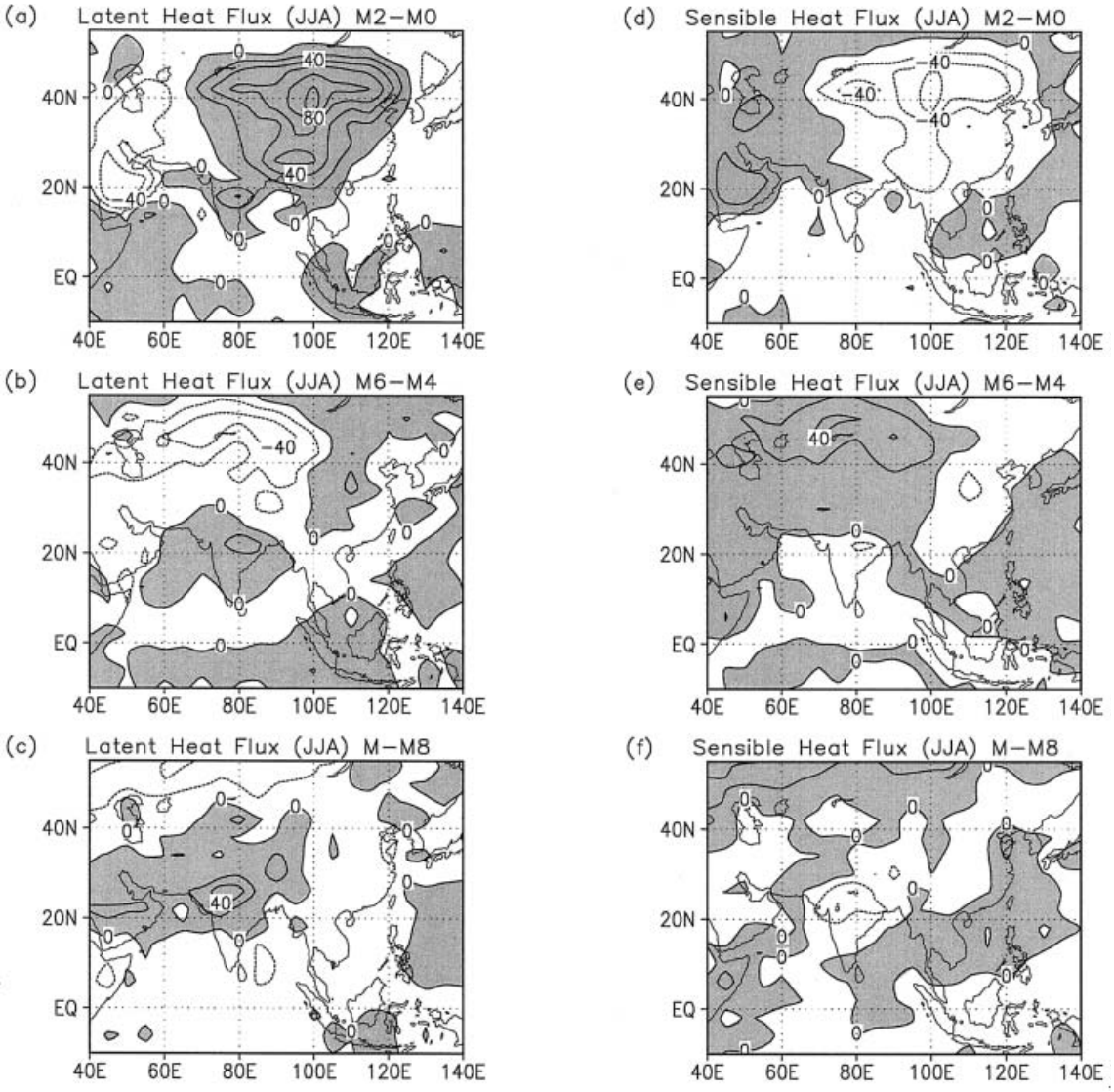

Fig. 11. Difference of seasonal mean latent and sensible heat flux at surface during June–August between (a) (d) M2 and M0, (b) (e) M6 and M4, and (c) (f) M and M8. Units are W m^{-2}. The positive values are shaded.

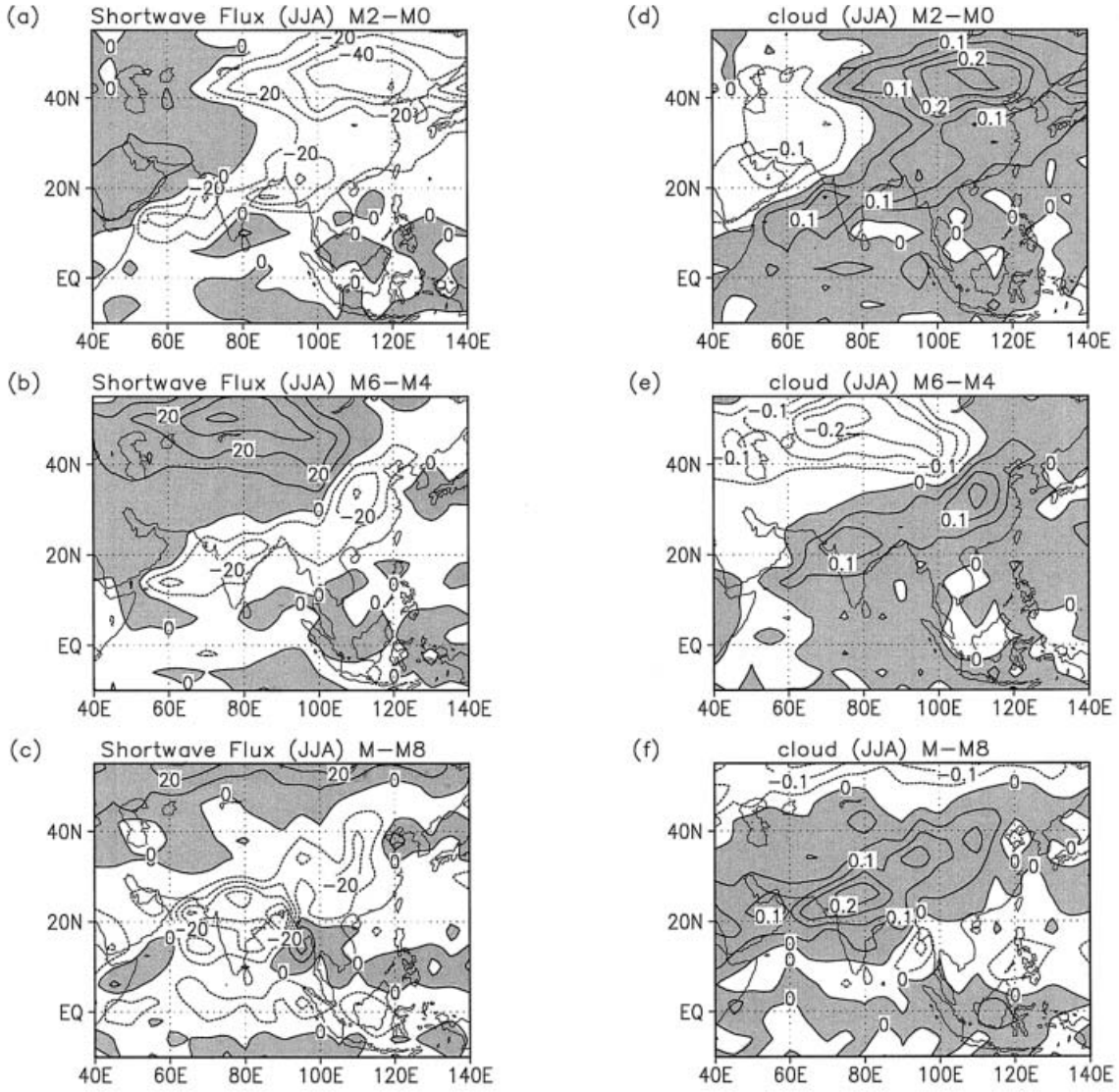

Fig. 12. Difference of seasonal mean shortwave radiation flux at surface and cloud amount during June–August between (a) (d) M2 and M0, (b) (e) M6 and M4, and (c) (f) M and M8. Units of shortwave radiation are W m^{-2}. The positive values are shaded.

agrees with the increase in ground wetness. From M6 to M, latent (sensible) heat flux over India increases (decreases), although these values are smaller than those in the earlier stages of mountain uplift. Further, shortwave radiation flux at surface over the moist Asia region decreases due to cloud increased with mountain uplift, as shown in Fig. 12. The decrease in shortwave radiation in East Asia is remarkable from M0 to M2 (Fig. 12a). In Central Asia, however, shortwave radiation increases with mountain uplift due to the decrease in cloud amount, particularly, in the later stages of the mountain uplift. In northern India, the large decrease in shortwave radiation appears from M8 to M (Fig. 12c).

Figure 13 shows the change of latent heat, sensible heat, shortwave radiation, and longwave radiation flux at surface with mountain uplift in India (75°E–80°E, 10°N–30°N), Southeast Asia (95°E–105°E, 10°N–30°N), East Asia (105°E–120°E, 30°N–45°N), and Central Asia

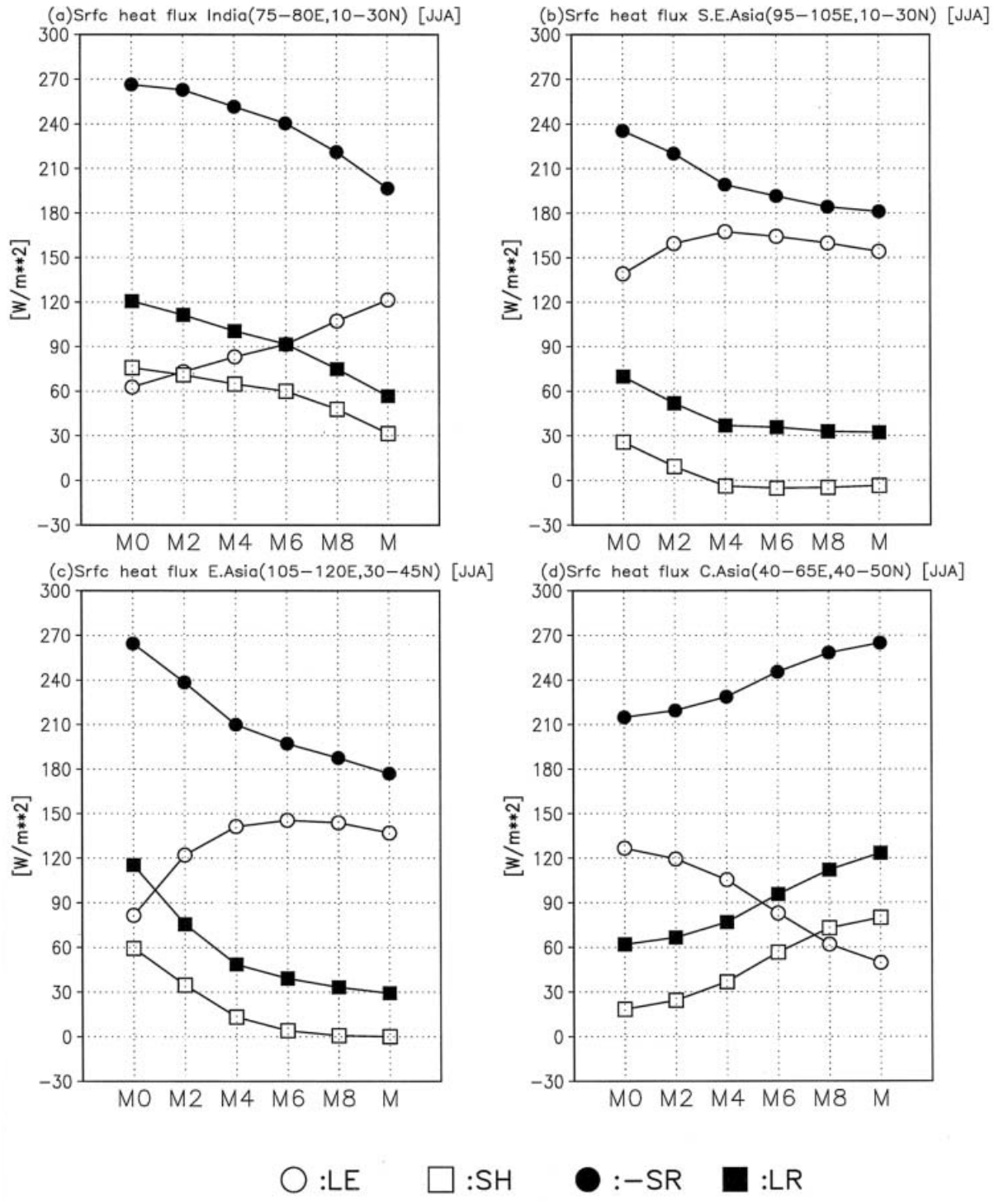

Fig. 13. The change of latent heat, sensible heat, shortwave radiation, and longwave radiation flux at surface with mountain uplift in (a) India (75°E–80°E, 10°N–30°N), (b) Southeast Asia (95°E–105°E, 10°N–30°N), (c) East Asia (105°E–120°E, 30°N–45°N), and (d) Central Asia (40°E–65°E, 40°N–50°N). Units are W m^{-2}. Open circle (square) indicates latent (sensible) heat flux at surface, and closed circle (square) indicates shortwave (longwave) radiation flux at surface. The positive values of shortwave radiation flux at surface indicate a downward direction, and that of other fluxes an upward direction.

(40°E–65°E, 40°N–50°N), respectively. The change of shortwave radiation flux with mountain uplift is consistent with that of cloud amount. In connection with the migration of the active convection region, latent heat flux over India increases gradually with mountain uplift, while sensible heat, shortwave radiation, and longwave radiation decrease. Shortwave radiation flux over Southeast and East Asia decreases with mountain uplift, particularly in the earlier stages of mountain uplift (Fig. 13b and Fig. 13c). Sensible heat and longwave radiation flux also decrease largely over Southeast and East Asia in the earlier uplift stages. These changes are consistent with the changes in the earlier uplift stages that ground wetness over Southeast and East Asia increases largely (Fig. 10), and that surface temperature decreases. The increase in shortwave radiation, longwave radiation and sensible heat flux over Central Asia begins to appear from M4 to M6 (Fig. 13d). These changes are outstanding in the later stages of mountain uplift, as well as the decrease in those fluxes over South and East Asia. Further, these changes are consistent with the change of ground (surface air) temperature and ground wetness.

These results stated above indicate surface air (ground) temperature is affected significantly by ground wetness and surface heat flux change induced by the increased precipitation. With mountain uplift, the decrease (increase) in shortwave radiation flux into surface (cloud amount) coincides with the increase of precipitation, as well as the increase in latent heat flux. Therefore, ground surface temperature over moist Asia decreases with mountain uplift due to the decrease in shortwave radiation into surface by cloud effect, and the wetter ground, in addition to the rise of ground surface.

3.3 SST change over the tropical Indian Ocean

Figure 14 shows SST in the Indian Ocean averaged within June–August in M0, M4, and M8 and its difference in M2, M6, and M8 from that in M0, respectively. In M0 (Fig. 14a), SST in the northern hemisphere is larger than 28°C. From M0 to M2 (Fig. 14b), SST over the Arabian Sea and the Bay of Bengal decreases due to the decrease in shortwave radiation flux into surface by cloud effect and the increase in latent heat flux (Fig. 12a). In M6 (Fig. 14d), SST in the Bay of Bengal also increases due to decreased shortwave radiation flux associated with the change of cloud amount. On the other hand, SST in the equatorial Indian Ocean increases with mountain uplift; particularly large increase is found in the eastern equatorial Indian Ocean. Although southerly wind at low-level across the equator in M0 is stronger over the eastern Indian Ocean, the southerly wind over the eastern equatorial Indian Ocean becomes weaker, and southerly wind over the western becomes stronger with mountain uplift. Thus, these changes are related to the weakness of the upwelling in the eastern Indian Ocean. The enhanced southerly wind over the western Indian Ocean causes the enhancement of upwelling in the western Indian Ocean, and a western part of the Arabian Sea. Further, the westerly component of sea surface wind stresses in the equatorial Indian Ocean becomes larger with mountain uplift. This change also causes the weakness of a sea surface current toward poleward, related to the increase in SST in the equatorial Indian Ocean. The increase in SST also results in the increase of precipitation in the equatorial Indian Ocean, as shown in Fig. 5. Both shortwave radiation flux, and latent heat flux in the equatorial Indian Ocean, decrease with mountain uplift. Therefore, the increase in SST in the equatorial Indian Ocean results from the change of the ocean dynamics. Using CGCM in this study, we can describe the increase of precipitation consistent with the increase in SST over the equatorial Indian Ocean, as well as the change in SST. In Chandrasekar and Kitoh (1998), the presence of positive SST anomalies south of the equator over the Indian Ocean resulted in the decrease in precipitation over Indian Ocean, and the weakening of the mean monsoon circulation. Therefore, the increase in SST in the equatorial Indian Ocean with mountain uplift must affect the change of the monsoon precipitation and circulation over South and East Asia. If using AGCM with observed SST, warmer SST in the equatorial Indian Ocean may affect the monsoon precipitation in M0. This result indicates that summer SST distribution in the Indian Ocean is affected significantly by the evolution of the Asian summer monsoon. The effect of mountain uplift should

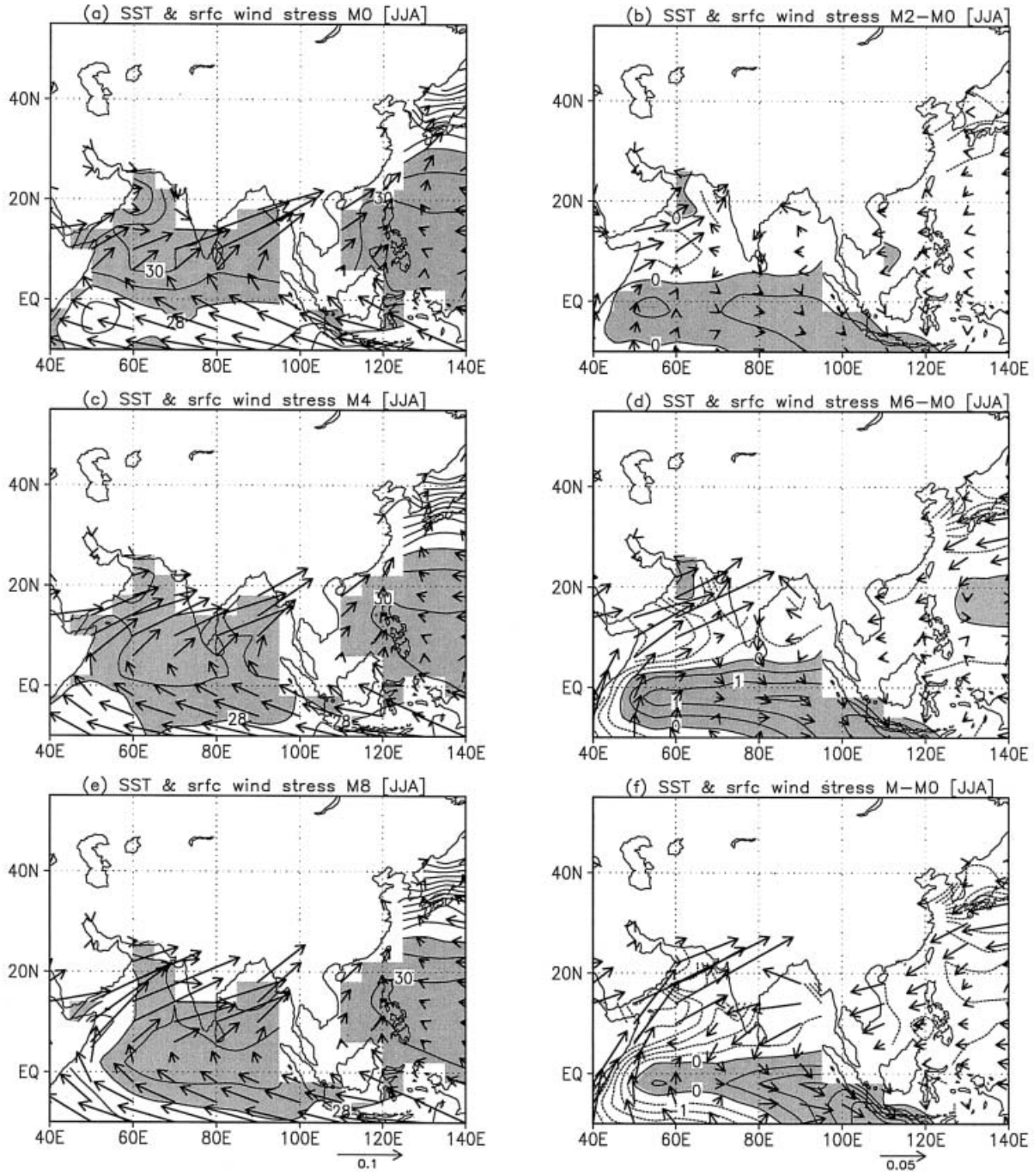

Fig. 14. Seasonal mean SST and surface wind stress in (a) M0, (c) M4 and (e) M8, and its difference during June–August between (b) M2 and M0, (d) M6 and M4, and (f) M and M8. Units of SST are °C and those of surface wind stress are N m^{-2}. Shaded area indicates the values above 28°C in (a), (c), and (e), and the positive values in (b), (d), and (f).

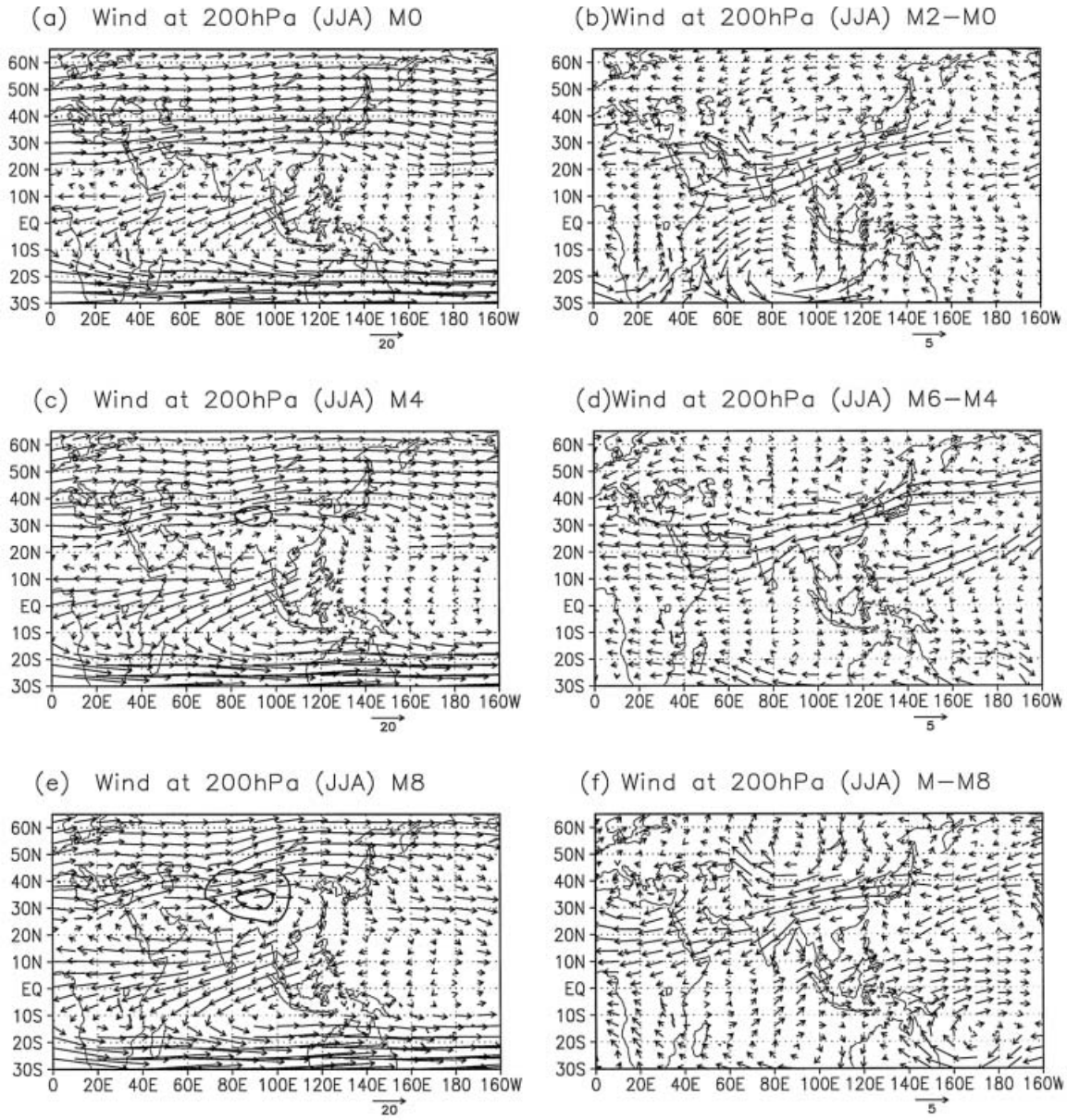

Fig. 15. (a) (c) (e) Seasonal mean distribution of wind at 200 hPa during June–August in M0, M4, and M8, and (b) (d) (f) the difference of wind at 200 hPa between M2 and M0, M6 and M4, and M and M8. Units are m s^{-1}. The contour shows mountain height at 1500 and 3000 m.

be investigated with coupled GCM including full ocean processes.

3.4 Upper-level atmospheric circulation

Wind distribution at 200 hPa in M0, M4, and M8, and its difference between M2 and M0, M6 and M4, and, M and M8 are shown in Fig. 15. In M0 (Fig. 15a), westerly is found zonally in the whole north of 30°N; particularly, an extreme flow called the subtropical jet exists at 30°N over Asia. There is also weak anticyclonic circulation linked with convective activity over South Asia. Further, over the equatorial Indian Ocean, northeasterly crossing the equator is found. The important change with mountain uplift for the circulation at 200 hPa is that anticyclonic circulation is enhanced, and becomes conspicuous over South Asia.

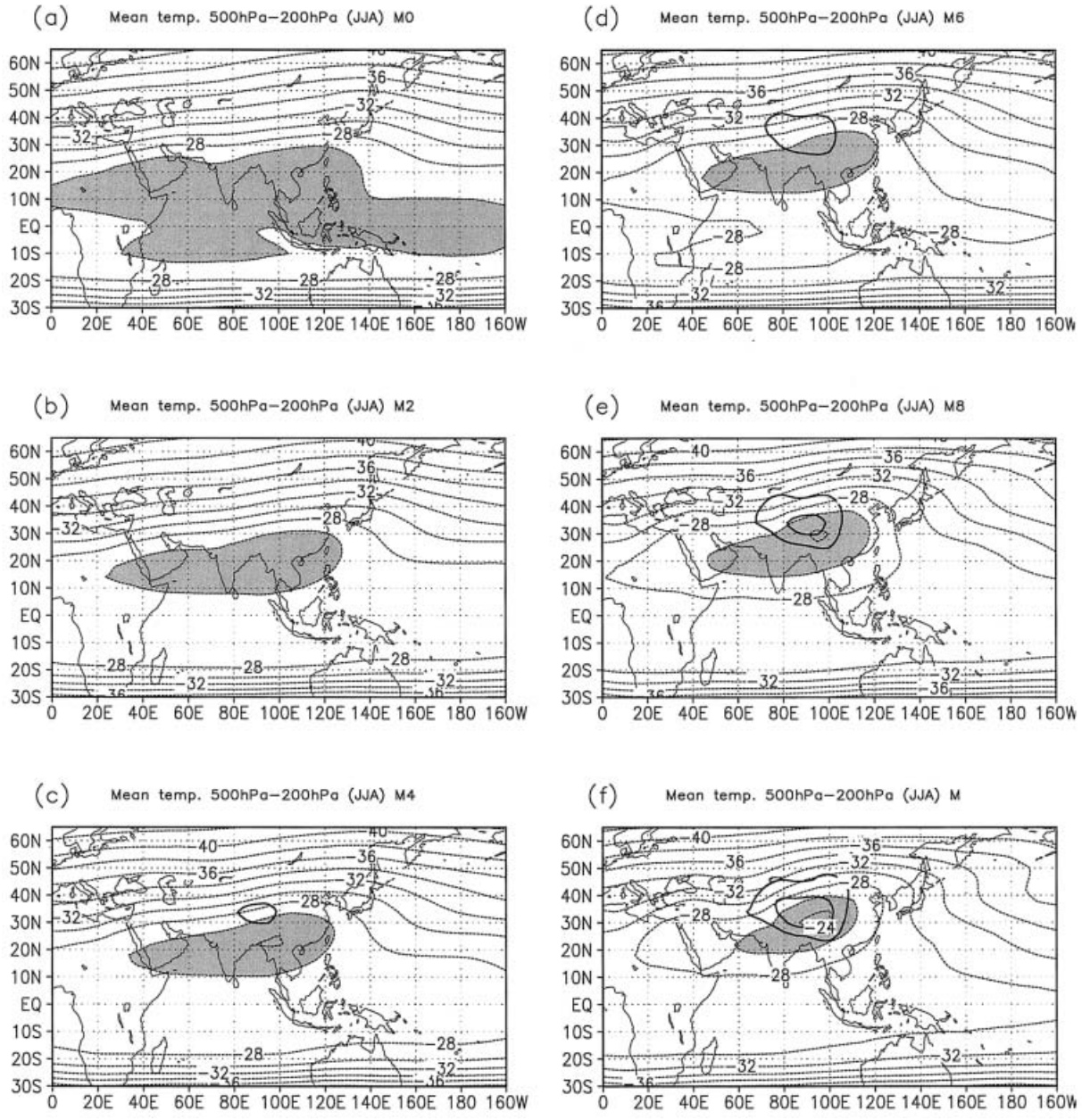

Fig. 16. Seasonal mean distribution of mean temperature between 500 hPa and 200 hPa during June–August in each run. Units are °C and the contour interval is 2°C. Temperature above −26°C are shaded. The thick contour shows mountain height at 1500 and 3000 m.

As shown by the wind difference between M2 and M0 in Fig. 15b, easterly is enhanced over South Asia and the equatorial Indian Ocean. As anticyclonic circulation anomalies are found over East Asia, and the South Indian Ocean, the anticyclonic circulation centered in Myanmar becomes more outstanding in M2. In M4, anticyclonic circulation over the whole of South Asia is enhanced. Thus, the subtropical jet is diverted north over East Asia, and the northeasterly over the equatorial Indian Ocean is stronger than that in M0.

Figure 16 shows the seasonal mean distribution of mean temperature between 500 hPa and

200 hPa during June–August, averaged for the last 30 years. In M0 (Fig. 16a), the temperature over the low latitude region is above −28°C. A warm area above −26°C in M0, also exits over South Asia and the North Indian Ocean, but the reversal of the meridional temperature gradient between the continents and the Indian Ocean is not distinguishable (Fig. 16a). Although the area above −26°C is smaller in M2 (Fig. 16b) and M4 (Fig. 16c) than in M0, the reversal of the temperature gradient from the equatorial Indian Ocean to South Asia, appears over South Asia. Figure 17 shows the change of the north-south and the east-west land-sea contrast of mean temperature between 500 hPa and 200 hPa, with mountain uplift. Figure 17a shows the difference of the temperature between 30°N and the equator, and Fig. 17b the difference between 90°E and 130°E. The north-south contrast over South Asia is negative in M0. The reversal of the contrast from negative to positive appears over the eastern continent in the earlier stages, the reversal is also found over the entire South Asia region in the later stages. The maximum north-south contrast exists in the earlier stages at about 110°E, but that in M8 and in M, it changes to 95°E. Particularly, the north-south contrast between the plateau and sea increases largely in the later stages. The east-west contrast over East Asia affects significantly East Asian monsoon. In M0, the east-west contrast of the temperature is smaller over East Asia, while the contrast over Southeast Asia is positive. In the earlier stages, the east-west contrast over Southeast Asia is enhanced. While a small change of the contrast is found from M4 to M6, that over East Asia becomes significantly stronger in the later stages.

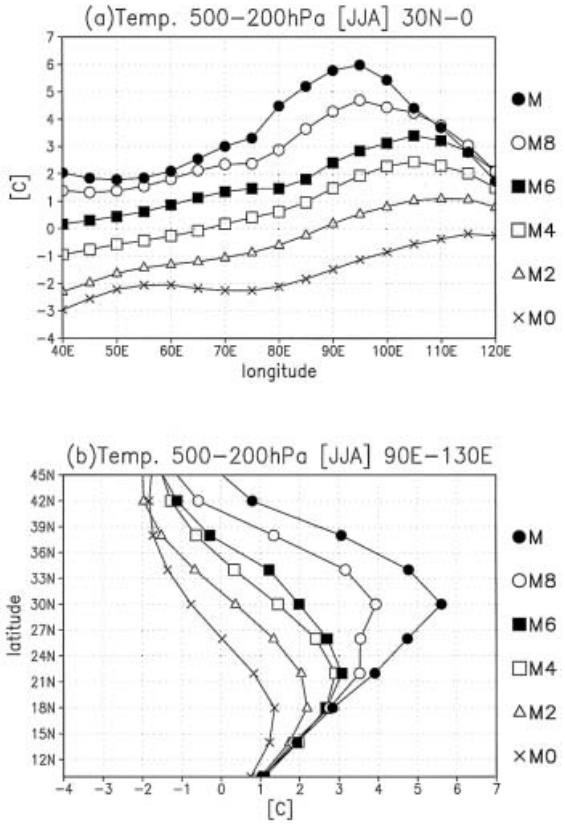

Fig. 17. Change of (a) the north-south and (b) west-east land-sea contrast of mean temperature between 500 hPa and 200 hPa with mountain uplift. (a) shows the difference of the temperature between 30°N and the equator, and (b) the difference between 90°E and 130°E. Units are °C.

The center of the anticyclonic circulation moves from about (100°E, 20°N) in M0 to about (90°E, 26°N) in M6. While the difference for the center of the anticyclonic circulation between M0 and M4 is not noticeable, that between the earlier stages (M0, M2, M4) and the later stages (M6, M8, M) is remarkable. Easterly anomalies over South and East Asia, shown in Fig. 15d and 15f, indicate that the anticyclonic circulation moves to the northwest. In the later stages of mountain uplift, therefore, the center of the anticyclonic circulation moves gradually to the top of the Tibetan Plateau. Moreover, as the anticyclonic circulation extends to Northeast Asia, the northerly is dominant over East Asia particularly in M8 and M. Over the ocean to the east of Japan, a westerly wind component also decreases from M6 and M, as shown in Fig. 15d and 15f.

In M8 (Fig. 16e), an area above −28°C appears only over South Asia, and then temperature above −24°C is found over the Tibetan Plateau. Therefore, the temperature gradient from the ocean to the land is outstanding over the Indian Ocean/South Asia compared with that in the earlier stages (M0-M4). The east-west temperature gradient is also found over East Asia and the northwestern Pacific. In M, the warmer area above −26°C is found centered over the Tibetan Plateau. Further, the

temperature gradient from the ocean to the warm center over the Tibetan Plateau, is noticeable in M compared with that in the earlier stages of mountain uplift.

Incidentally, the subtropical jet is diverted and becomes weaker by the development of the anticyclonic circulation with mountain uplift. Flows crossing the equator over the Indian Ocean are enhanced in consistent with the enhancement of the anticyclonic circulation in the earlier stages (Fig. 15b), while a remarkable change of the circulation in M6 and M8 is not found (Fig. 15d and 15f). However, the northeasterly becomes weaker over the eastern Indian Ocean, and the maritime continent in M.

4. Intensity of the Asian summer monsoon

As shown by figures used in the previous section, the various local changes of some meteorological components are found with progressive mountain uplift. In this section, change in the intensity of the Asian summer monsoon is focused on, using four indices shown in Fig. 18. They are: the seasonal mean precipitation during June–August averaged in India (75°E–80°E, 10°N–30°N) (IMR), in Southeast Asia (95°E–105°E, 10°N–30°N) (SEA), and in East Asia (105°E–120°E, 30°N–45°N) (EA), and the seasonal mean zonal wind shear between 850 hPa and 200 hPa during June–August averaged in an area (40°E–100°E, 2°N–18°N) as defined in Webster and Yang (1992) (WYI).

The abscissa in this figure indicates the stage of mountain uplift. The intensity of the Asian summer monsoon indicated by IMR increases from M0 to M. Moreover, the increase rate from M0 to M6 is a half of that from M6 to M. While the migration of the active convection region over India is slower in the earlier stages of mountain uplift, that is faster in the later stages. The standard deviation of the interannual variability of IMR also increases with mountain uplift. SEA index indicates the enhancement in the earlier stages of mountain uplift and the weakening in the later stages. Also, the EA index shows weak enhancement in the later stages of mountain uplift, compared with enhancement in the earlier stages. From M0 to M4, the precipitation area extends largely in the land of South and East Asia and then precipitation increases in the Arabian Sea, the Bay of Bengal and India, as stated in the previous section (Fig. 4). While the increase in precipitation over the slope of the Tibetan Plateau and India occurs from M6 to M, precipitation decreases in the southern part of the Bay of Bengal and the Indochina Peninsula. The large increase in precipitation are also restricted in a smaller area over the northern part of the Arabian Sea, India and the slope of the Tibetan Plateau in the later stages of mountain uplift. Therefore, the enhancement of SEA and EA index in the earlier stages of mountain uplift is consistent with the increase and the areal expansion of large precipitation over Southeast and East Asia. Further, the decrease in precipitation over the coastal region of Southeast East Asia is associated with the weakening of SEA and the weaker enhancement of EA in the later stages. However, the increase in the standard deviation of their interannual variability is small compared with IMR and WYI.

The intensity of the Asian summer monsoon indicated by the WYI is shown in Fig. 18d. The Asian summer monsoon becomes strong from M0 to M8 as well as that indicated by EA. Also, the standard deviation of its interannual variability increases with mountain uplift. The large enhancement of WYI occurs from M0 to M6, compared with that from M6 to M8, which differs from the enhancement indicated by IMR. From M0 to M6, westerly wind speed at 850 hPa increases over the Arabian Sea, India and the Bay of Bengal. However, weakened westerly at 850 hPa is found over the Bay of Bengal and the Indochina Peninsula from M6 to M in association with the northward migration of southwesterly, as stated in the previous section. At 200 hPa, the easterly is enhanced over the whole of South Asia and the North Indian Ocean, with progressive mountain uplift. Thus, the weak enhancement of the Asian summer monsoon in the later stages of mountain uplift results from the weakened westerly at low-level over the Bay of Bengal and the Indochina Peninsula.

The changes of the Asian summer monsoon, with progressive mountain uplift, based upon the changes of four indices. The Indian summer monsoon becomes strong with mountain uplift.

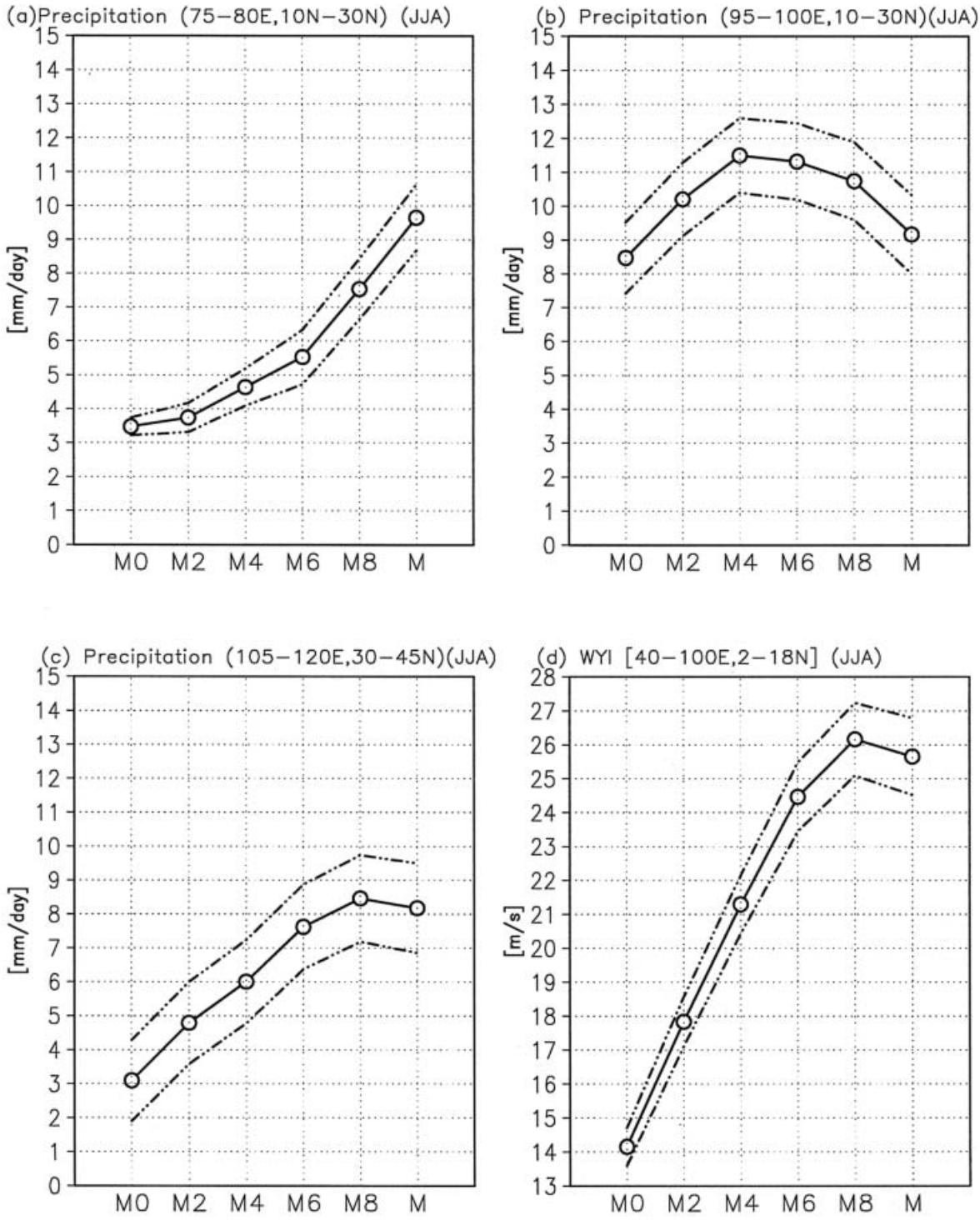

Fig. 18. Indices of the Asian summer monsoon: the seasonal mean precipitation during June–August averaged in (a) India (75°E–80°E, 10°N–30°N) (IMR), in (b) Southeast Asia (95°E–105°E, 10°N–30°N) (SEA), and in (c) East Asia (105°E–120°E, 30°N–45°N) (EA). (d) The seasonal mean zonal wind shear between 850 hPa and 200 hPa during June–August averaged in an area (40°E–100°E, 2°N–18°N) as defined in Webster and Yang (1992) (WYI). The abscissa in this figure indicates the stage of the mountain uplifts. The dot-dot-dash line indicates the standard deviation of the interannual variability in each stage.

Also, the Indian sumer monsoon in the later stages of mountain uplift shows great enhancement, and the migration into northern India of an active convection region remarkably occurs. On the contrary, the monsoon circulation indicated by WYI, becomes even weaker from M8 to M, as decreased precipitation and weakened monsoon westerly at low level appear in South and Southeast Asia. The enhancement of the East Asian monsoon with mountain uplift is similar to that of the large-scale monsoon circulation defined by WYI index. In Southeast Asia, however, the monsoon is the strongest in about a half mountain stage, unlike the Indian and East Asia monsoon. In Liu and Yin (2002), the change of the intensity of the Indian, Southeast Asian, and Northeast Asian monsoon with mountain uplift were investigated using the indices based on the seasonal change of an averaged surface wind direction and velocity between summer and winter. The change of the Southeast Asian monsoon with mountain uplift in their study is similar to that in this study. In their study, however, the enhancement of the Indian monsoon was not found.

5. Concluding remarks

Rainfall, and low-level westerly representing the Asian summer monsoon, appear in M0 which has land-sea distribution, but without orography. Weak anticyclonic circulation is also found at the upper-level over the north Indian Ocean in M0. There is northward expansion of an active convection region, and the monsoon westerly over South Asia, clearly in the earlier stages of mountain uplift. Thus, the moist climate region appears over South and East Asia, even in the lower, than a half of the present mountain case, while a dry climate region is found over Iran-Afghanistan region, as is in the present. In M0, precipitation over South Asia is concentrated at about 10°N and quite large. In the earlier stages of mountain uplift, precipitation over South, Southeast and East Asia increases quantitatively. Its region migrates northward spatially, with mountain uplift. In the later stages of mountain uplift, precipitation migrates largely into the south and southeastern slope of the Tibetan Plateau and North India, but decreases particularly in the Bay of Bengal and the Indochina Peninsula. In association with the quantitative and spatial change in precipitation, ground wetness increases largely in the earlier stages of mountain uplift, in which the dry ground surface in M0 becomes wet ground surface over South and East Asia. These changes change surface heat flux in the land over Southeast and East Asia significantly in the earlier stages. However, in the later stages of mountain uplift, ground wetness, and surface heat flux have smaller changes, because the wetter ground surface already has presented over Southeast and East Asia, under the condition with the mountain height lower than the half. Ground temperature also decreases further due to the wetter ground surface and the decrease in shortwave radiation into surface by cloud effect, in addition to the rise of ground surface. Further, SST in the Arabian Sea and the Bay of Bengal, decreases with mountain uplift, due to the reduction of shortwave radiation by cloud effect and the increase in latent heat flux. These changes with mountain uplift also contribute to suppress the fall of pressure, or to raise pressure over South Asia and East Asia. Therefore, while westerly is accelerated further in the inland side of South and Southeast Asia, that is weakened with mountain uplift in the ocean side, consistent with the weekend monsoon westerly over the Bay of Bengal and the Indochina Peninsula. As a result, southwesterly in Southeast and East Asia migrates northwestward into the interior with mountain uplift, and precipitation decreases over the coastal region in Southeast and East Asia. The northwestward movement of southwesterly in Southeast and East Asia may also be affected by the enhanced subtropical high with mountain uplift.

The north-south temperature contrast at middle-upper level between the land and the sea over South Asia is smaller in the earlier stages of mountain uplift. In the later stages, the contrast, particularly, over an area including the Tibetan Plateau, becomes large. The west-east temperature contrast at middle-upper level over Southeast Asia appears in the earlier stages. However, the contrast over East Asia becomes large with mountain uplift. In M8 and M, the maximum contrast is also found at 30°N.

The intensity of the Indian, Southeast Asian, and East Asian monsoon was investigated with

indices which were defined by area mean precipitation. Indian monsoon becomes strong gradually with mountain uplift; particularly in the later stages its remarkable enhancement is found. This result differs from the result in Liu and Yin (2002). The intensity of Southeast Asian monsoon is the strongest in M4. Thus, in the later stages of mountain uplift, that becomes weaker in association with the northward migration of convective activity. Although East Asian monsoon is enhanced gradually with mountain uplift, the enhancement in the earlier stages is larger than that in the later stages. Results in Liu and Yin (2002) showed that Southeast Asia monsoon has intensified during 0%–70% of the present mountain, but weakened during 70%–100%. Their result is similar to our result. However, since their indices were defined by the seasonal change of surface wind between summer and winter, our indices are different from theirs. Further, their experiments using AGCM is essentially different from ours using CGCM. In the equatorial Indian Ocean, SST also increases with mountain uplift, resulting in the increase in precipitation. The increase in SST results from the change of the ocean surface dynamics due to the enhanced monsoon circulation, and that could not be obtained if CGCM was not used in this study.

In this study, the height of global orography changed in each run. The results in this study, therefore, also include the effect of mountains besides the Tibetan Plateau. As the high terrain in the eastern African continent is related to the evolution of the Somali jet, the jet may be enhanced not only by the Tibetan Plateau uplift, but also by the high terrain. The enhanced subtropical high with global mountain uplift also influences the Asian monsoon circulation. In particular, the Rocky mountains also enhance the subtropical high over the North Pacific (Hoskins 1996; Rodwell and Hoskins 2001). To investigate the sole effect of Tibetan Plateau and the Rocky mountains separately, we are performing other experiments.

The quantitative and spatial changes of a climate by mountain uplift may depend significantly on physical processes (e.g., the parameterization of cumulus convection) in the model. Precipitation, for example, shows large variety among GCMs in the world (Gadgil and Sajani 1998; Kang et al. 2002), depending upon different parameterization of cloud/precipitation processes. Therefore, experiments using different models and/or schemes may be required in order to understand more comprehensively the climate changes associated with mountain uplift.

Acknowledgments

The authors are grateful to Dr. F. Kimura, Dr. H.L. Tanaka, Dr. H. Ueda, and graduate students in the climatology and meteorology group in the University of Tsukuba for their valuable advice. We also thank two anonymous reviewers for their valuable comments. This work was done as a co-operative study between the Institute of Geoscience, University of Tsukuba and the Meteorological Research Institute. It was also partially supported by Large Scale Numerical Simulation Project of Science Information Processing Center, University of Tsukuba.

References

Broccoli, A.J. and S. Manabe, 1992: The effects of orography on middle latitude northern hemisphere dry climate. *J. Climate*, **5**, 1181–1201.

Chandrasekar, A. and A. Kitoh, 1998: Impact of localized sea surface temperature anomalies over the equatorial Indian Ocean on the Indian summer monsoon. *J. Meteor. Soc. Japan*, **76**, 841–853.

Gadgil, S. and S. Sajani, 1998: Monsoon precipitation in the AMIP runs. *Clim. Dyn.*, **14**, 659–689.

Hahn, D.G. and S. Manabe, 1975: The role of mountains in the south Asian monsoon circulation. *J. Atmos. Sci.*, **32**, 1515–1541.

Hoskins, B., 1996: On the existence and strength of the summer subtropical anticyclones. *Bull. Amer. Meteor. Soc.*, **77**, 1287–1292.

Kang, I.S., K. Jin, B. Wang, K.M. Lau, J. Shukla, V. Krishnamurthy, S.D. Schubert, D.E. Waliser, W.F. Stern, A. Kitoh, G.A. Meehl, M. Kanamitsu, V.Y. Galin, V. Satyan, C.K. Park and Y. Liu, 2002: Intercomparison of the climatological variations of Asian summer monsoon precipitation simulated by 10 GCMs. *Clim. Dyn.*, **19**, 383–395.

Kitoh, A., 1997: Mountain uplift and surface temperature changes. *Geophys. Res. Lett.*, **24**, 185–188.

———, 2002: Effect of large-scale mountains on

surface climate—A coupled ocean-atmosphere general circulation model study—. *J. Meteor. Soc. Japan*, **80**, 1165–1181.

———, S. Yukimoto and A. Noda, 1999: ENSO-monsoon relationship in the MRI coupled GCM. *J. Meteor. Soc. Japan*, **77**, 1221–1245.

———, A. Noda, Y. Nikaidou, T. Ose and T. Tokioka, 1995: AMIP simulations of the MRI GCM. *Pap. Meteorol. Geophys.*, **45**, 121–148.

Kutzbach, J.E., P.J. Guetter, W. Ruddiman and W.L. Prell, 1989: Sensitivity of climate to Late Cenozoic uplift in southern Asia and the American West: numerical experiments. *J. Geophys. Res.*, **94**, 18393–18407.

———, W.L. Prell and W.F. Ruddiman, 1993: Sensitivity of Eurasian climate to surface uplift of the Tibetan Plateau. *J. Geology*, **101**, 177–190.

Lacis, A.A. and J.E. Hansen, 1974: A parameterization for the absorption of solar radiation in the Earth's atmosphere. *J. Atmos. Sci.*, **31**, 118–133.

Liu, X. and Z.-Y. Yin, 2002: Sensitivity of East Asia monsoon climate to the uplift of the Tibetan Plateau. *Palaeogeog., Palaeoclimat., Palaeoecol.*, **183**, 223–245.

Manabe, S. and T.B. Terpstra, 1974: The effects of mountains on the general circulation of the atmosphere as identified by numerical experiments. *J. Atmos. Sci.*, **31**, 3–42.

Nagai, T., T. Tokioka, M. Endoh and Y. Kitamura, 1992: El Nino-Southern Oscillation simulated in an MRI atmosphere-ocean coupled general circulation model. *J. Climate*, **5**, 1202–1233.

Palmer, T.N., G.J. Shutts and R. Swinbank, 1986: Alleviation of a systematic westerly bias in general circulation and numerical weather prediction models through an orographic gravity wave drag parameterization. *Quart. J. Roy. Meteor. Soc.*, **112**, 1001–1039.

Rodwell, M.J. and B.J. Hoskins, 2001: Subtropical anticyclone and summer monsoons. *J. Climate*, **14**, 3192–3211.

Shibata, K. and T. Aoki, 1989: An infrared radiative scheme for the numerical models of weather and climate. *J. Geophys. Res.*, **94**, 14923–14943.

Tokioka, T. and A. Noda, 1986: Effects of large-scale orography on January atmosphere circulation: A numerical experiment. *J. Meteor. Soc. Japan*, **64**, 819–840.

———, K. Yamazaki, A. Kitoh and T. Ose, 1988: The equatorial 30–60 day oscillation and the Arakawa-Schubert penetrative cumulus parameterization. *J. Meteor. Soc. Japan*, **66**, 883–901.

Webster, P.J. and S. Yang, 1992: Monsoon and ENSO: Selectively interactive systems. *Quart. J. Roy. Meteor. Soc.*, **118**, 877–926.

Yasunari, T., 1990: Impact of Indian monsoon on the coupled atmosphere/ocean system in the tropical Pacific. *Meteorol. Atmos. Phys.*, **44**, 29–41.

Yukimoto, S., M. Endoh, Y. Kitamura, A. Kitoh, T. Motoi, A. Noda and T. Tokioka, 1996: Interannual and interdecadal variabilities in the Pacific in an MRI coupled GCM. *Clim. Dyn.*, **12**, 667–683.